



Proper flying capacitor selection for performance enhancement of five-level hybrid active neutral-point-clamped inverters

Samer Saleh Hakami¹ · Kyo-Beum Lee¹

Received: 18 May 2022 / Revised: 10 August 2022 / Accepted: 11 August 2022 / Published online: 29 August 2022
© The Author(s) under exclusive licence to The Korean Institute of Power Electronics 2022

Abstract

Flying capacitors (FCs) are very important in multilevel inverter systems when it comes to synthesizing additional voltage levels for various medium-voltage industrial applications, including renewable energy, motor drives, and power transmission. In particular, they are responsible for forming the five-level output pole voltages in five-level hybrid active neutral-point-clamped (ANPC) topologies. This is only possible when the FCs reach their reference values (i.e., 25% of the DC-link value). When a five-level hybrid ANPC inverter operates in the high-frequency (HF) range, the output three-phase current waveforms are less distorted when compared to the low-frequency (LF) performance. Instantaneously achieving a five-level output pole voltage during HF operation is a challenging task. This is due to the large capacitance of some existing types of FCs. In this study, a novel analysis of the effects of a FC on the performance of a five-level hybrid ANPC inverter is presented with simulation and experimental validations. Film capacitors significantly enhanced system performance when compared to electrolytic capacitors due to their many advantageous features, including the ability to charge and discharge quickly during HF operation. In addition, the total harmonic distortion of the output pole voltage is significantly suppressed. Consequently, the size of the required filter can be reduced. Therefore, the proposed system is highly desirable for various industrial applications.

Keywords Five-level hybrid ANPC inverter · Flying capacitor · HF operation · Multilevel inverters

1 Introduction

In recent decades, multilevel converters have been studied and applied in various medium-voltage industrial applications, including renewable energy, motor drives, and power transmission, owing to their high power density, high power quality, low dv/dt , and low voltage stress in the switches [1–5]. Among these converters are neutral-point-clamped (NPC) inverters, which do not require flying capacitors (FCs) or isolated DC-link sources when compared to cascaded H-bridge multilevel inverters [6]. However, the number of diodes increases when the output voltage level increases. As a result, a large number of passive switches can lead to unevenly distributed switching losses and reduced inverter efficiency.

To address the above-mentioned drawbacks, hybrid NPC inverters have been recently reported in the literature and employed in some industries [7–11]. The five-level hybrid active neutral-point-clamped (ANPC) inverter topology was first proposed in [12]. This topology has attracted considerable attention since it requires fewer active switching devices and fewer FCs. It was built as an extension of the well-known three-level hybrid active NPC inverter with the inclusion of two additional active switches, which results in a total of eight active switches, and one FC per phase, as shown in Fig. 1 [13–15].

However, in this topology, the voltage stresses in the switches are unequal [16–18]. Switching devices (S_{x1-4} , $x = a, b, \text{ or } c$ phase) must bear half of the applied DC-link voltage to form the five-level output voltage. This becomes a major challenge in medium-voltage applications unless double-switching devices are connected in series. Nevertheless, this results in a voltage-sharing problem [19].

To resolve this issue, S_{x1-4} needs to be controlled at the fundamental frequency (50 or 60 Hz), whereas the

✉ Kyo-Beum Lee
kyl@ajou.ac.kr

¹ Department of Electrical and Computer Engineering, Ajou University, Suwon, Republic of Korea

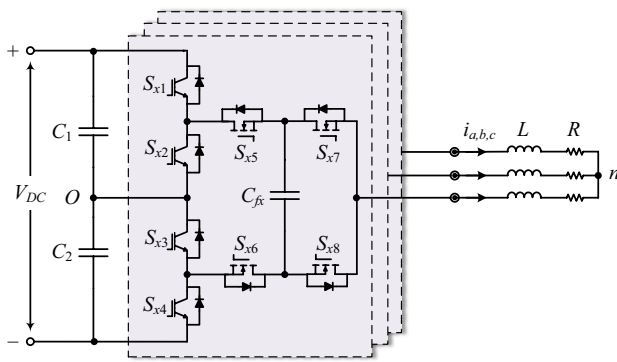


Fig. 1 Circuit topology of a five-level hybrid ANPC inverter

switching devices S_{x5-8} can be controlled at a higher switching frequency.

Various pulse width modulation (PWM) techniques have been reported to control five-level hybrid ANPC inverters, such as selective-harmonics-elimination PWM (SHE-PWM) [20], phase-disposition PWM (PD-PWM) [21], and phase-shift PWM (PS-PWM) [22]. Although SHE-PWM has the ability for voltage balancing across the FCs, it is very complex and requires a predefined lookup table to store the appropriate angles, which can lead to a slow-response control [20]. In contrast, the PD-PWM modulation technique offers a very fast response control with a low computational burden when compared to SHE-PWM [21]. However, it produces a more distorted output voltage in the five-level hybrid active NPC inverter with non-uniformly distributed switching and conducting losses. The PS-PWM modulation technique is capable of naturally balancing the FCs when compared to the PD-PWM modulation technique [22]. Consequently, a five-level output pole voltage is formed. However, the charging and discharging capabilities of the FCs are critical for high-frequency (HF) modulation.

A few methods have been reported in the literature for capacitor charging and discharging. However, they have the following issues. (1) High-voltage switching and high-voltage resistance are required for pre-charging the capacitor through the main circuit, which increases the system size and complexity. (2) Overvoltage can occur in the switching devices due to the charging of the capacitor bus. Then the voltage across the FC is controlled by the modulation technique to slowly charge and discharge the FC. An FC self-pre-charging approach was proposed in [23] to transfer the main circuit into a booster to charge the FCs to their reference values in the back-to-back five-level hybrid ANPC topology without the need for external hardware. However, the possibility of doubling the voltage stress on some of the switching devices increases dramatically.

Generally, the DC link of an inverter topology utilizes aluminum electrolytic capacitors or film capacitors.

Aluminum electrolytic capacitors are preferred for applications that requiring minimal DC-link voltage ripples since they have higher capacitance-to-volume ratios. However, they have an extremely high equivalent series resistance (ESR) and a very low ripple current rating [24]. Their ESR values are significantly influenced by the voltage amplitude, frequency, and operating temperature [24]. In contrast, film capacitors have very low ESR values and higher root mean square (RMS) current ratings, which allows them to operate at higher voltage levels. These features make their lifespans longer than those of electrolytic capacitors. Therefore, they are well suited for various applications where currents and voltage ripples are high at the DC link.

A novel analysis of the effects of FC size and type on the performance of a five-level hybrid ANPC inverter is presented in this paper. A detailed calculation of the FC size is shown for operating inverters in the HF range (i.e., ≥ 30 kHz) to maintain a low harmonic distortion. Both electrolytic and film capacitors are compared during low-frequency (LF) and high-frequency HF operation of the five-level hybrid ANPC inverter under the PS-PWM modulation scheme, which has the natural balancing capability of FCs.

The rest of this paper is organized as follows. Section 2 presents the structure of a five-level hybrid ANPC inverter along with its operational principle and PS-PWM modulation scheme. The effect of FC size and type on the performance of the five-level hybrid ANPC inverter is explained in Sect. 3. Sections 4 and 5 present extensive simulation results and experimental validations, respectively. Finally, Sect. 6 concludes the paper.

In this section, the structure of the five-level hybrid ANPC inverter, its operational principle, and the PS-PWM modulation technique are extensively detailed.

2 Five-level hybrid ANPC inverter

2.1 Structure and operational principle

As shown in Fig. 1, the circuit topology of a three-phase five-level hybrid ANPC inverter mainly consists of twelve Si insulated-gate bipolar transistors (IGBTs, S_{x1-4}), twelve SiC metal-oxide-semiconductor field-effect transistors (MOSFETs, S_{x5-8}), two DC-link capacitors (C_1 and C_2), and three FCs (C_{fx}). The main advantage of this topology is its simple structure, since it requires fewer switching devices and two DC-link capacitors with a better switching loss distribution when compared to the other five-level topologies.

This inverter operates at two different frequencies, the fundamental frequency for S_{x1-4} and the PWM switching frequency for S_{x5-8} . Therefore, to operate this topology at high PWM switching frequencies, SiC-MOSFETs are regarded as suitable choices for S_{x5-8} , and Si-IGBT devices

are recommended for S_{x1-4} . This structure can have excellent performance with minimized switching losses when compared to using all Si-IGBTs. In addition, it is cost-effective when compared with all SiC-MOSFET topologies [7]. In addition, this topology requires only two capacitors for the DC-link voltage (V_{DC}), which are separated by a neutral point and a single C_{fx} per phase.

C_{fx} needs to be charged and discharged within an allowable range that is close to its reference value, which is 1/4 of the applied V_{DC} . This can be achieved by the PS-PWM modulation scheme, which can control the switching states of the five-level hybrid ANPC inverter, as illustrated in Table 1. S_{x1} and S_{x3} work in a manner that is complementary to S_{x2} and S_{x4} , respectively. Similarly, S_{x5} and S_{x7} switch in a manner that is complementary to S_{x6} and S_{x8} , respectively.

There are eight possible switching states for the five-level hybrid ANPC inverter, as shown in Fig. 2. Switching states I–IV are responsible for forming the half-positive cycle of the output pole voltage V_{xn} . Meanwhile, the negative-half cycle

is generated from switching states V–VIII. From Table 1 and Fig. 2, switching states II–III and VI–VII are responsible for the charging and discharging of C_{fx} , respectively. Switching states III–VI are responsible for controlling the V_{DC} across the neutral point.

2.2 PS-PWM switching scheme based on offset voltage injection

Unlike the other modulation schemes used to control five-level hybrid ANPC inverters, PS-PWM is one of the best candidates owing to its robust and natural ability to balance the voltage across C_{fx} . In addition, the switching losses are equally distributed among all the switching devices due to the ability of SiC-MOSFETs to operate with minimum switching losses at HF. First, the three-phase reference pole voltages (V_{xn}^*) must be generated by injecting an offset voltage (V_{sn}), which switches at three times the line frequency (i.e., the fundamental frequency), as shown in Fig. 3. This allows for the extension of the modulation index (MI) by 15.5% and improves the total harmonic distortion (THD) [25].

Therefore, V_{xn}^* can be expressed as in (1):

$$V_{xn}^* = V_{xs}^* + V_{sn} \tag{1}$$

where V_{xs}^* is the reference phase voltage, and V_{sn} is the offset voltage, which can work as a third-harmonic injected triangle-wave signal, and can be calculated as in (2):

$$V_{sn} = -\left(\frac{V_{max} + V_{min}}{2}\right) \tag{2}$$

Table 1 Switching states of a five-level hybrid ANPC inverter

S_{x1}	S_{x5}	S_{x7}	Switching state	V_{xn}
1	1	1	I	$V_{DC}/2$
1	1	0	II	$V_{DC}/4$
1	0	1	III	$V_{DC}/4$
1	0	0	IV	0
0	1	1	V	0
0	1	0	VI	$-V_{DC}/4$
0	0	1	VII	$-V_{DC}/4$
0	0	0	VIII	$-V_{DC}/2$

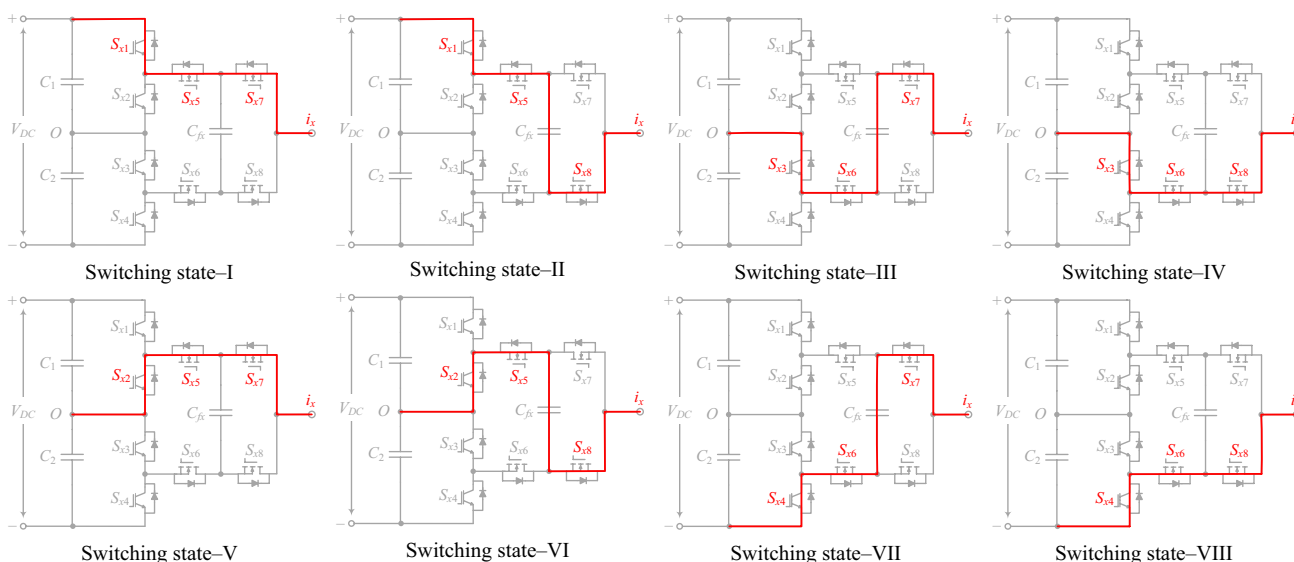


Fig. 2 Eight switching states of five-level hybrid ANPC inverter

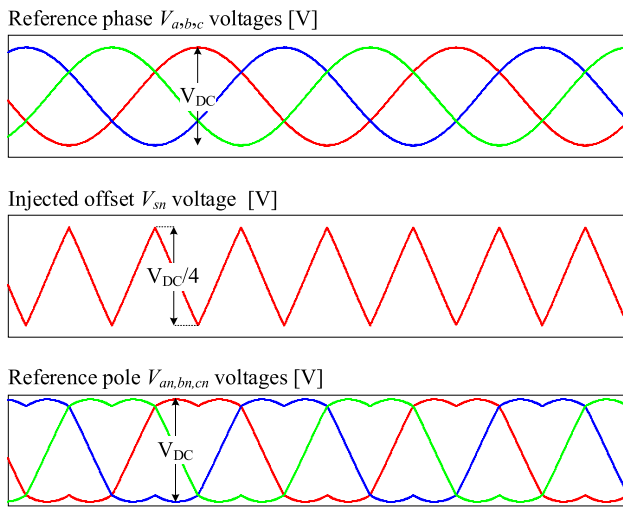


Fig. 3 Process for generating reference three-phase pole voltages

where V_{max} and V_{min} denote the maximum and minimum values of the three-phase reference voltages, respectively.

To satisfy the requirements for generating V_{xn} , two PWM carriers must be included in the PS-PWM switching scheme, with a 180° phase shift. As mentioned in the previous subsection, the switching principle for Si-IGBT switching devices (S_{x1-4}) depends on the reference signal. Therefore, they are switched in the same manner as the fundamental frequency, which is either 50 Hz or 60 Hz, depending on the country. Hence, the switching rules are given by (3):

$$S_{x1}, S_{x3}, \bar{S}_{x2}, \text{ and } \bar{S}_{x4} = \begin{cases} 1, & T_x < 1 \\ 0, & T_x \geq 1 \end{cases} \quad (3)$$

where T_x represents the reference signal.

Similarly, the SiC-MOSFET switching devices S_{x5-8} are turned ON and OFF in a complementary manner by comparing the normalized reference signals ($T_{x_normalized}$) with the PWM carriers, as shown in Fig. 4, which is expressed as in (4).

$$S_{x5} \text{ and } \bar{S}_{x6} = \begin{cases} 1, & T_{x_normalized} \geq \text{PWM carrier 1} \\ 0, & T_{x_normalized} < \text{PWM carrier 1} \end{cases} \quad (4)$$

$$S_{x7} \text{ and } \bar{S}_{x8} = \begin{cases} 1, & T_{x_normalized} \geq \text{PWM carrier 2} \\ 0, & T_{x_normalized} < \text{PWM carrier 2} \end{cases}$$

Moreover, this switching scheme ensures that a five-level output voltage can be generated with a balanced voltage across C_{fx} as well as the DC-link capacitors C_1 and C_2 .

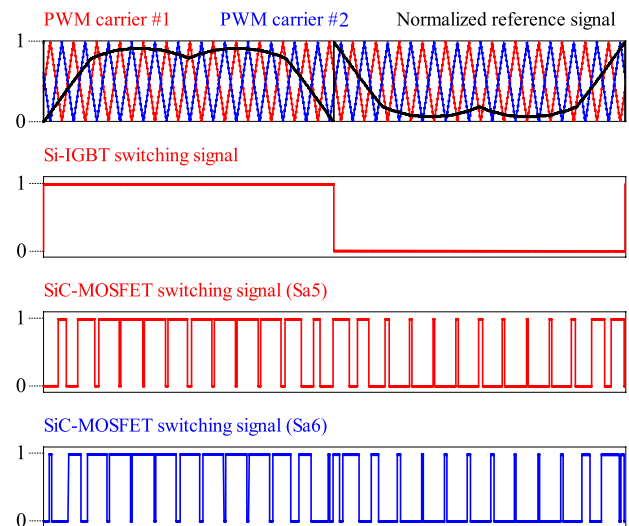


Fig. 4 Working principle of PS-PWM in generating output switching signals

3 FC influence on five-level hybrid ANPC inverter performance

Figure 5 shows a comparison of different types of capacitors. Capacitors may be suitable for high-voltage or high-capacity applications, depending on the dielectric material. Capacitors made from ceramics and electrolytes are mainly used in power electronic applications owing to their high voltage and capacitance. Polymer films, as dielectric materials, are often used on offshore platforms as capacitors with different types of dielectrics. Capacitors based on polymer films exhibit excellent self-healing characteristics and have a reasonable cost [27]. Thus, film capacitors are considered to be a good candidates for use as FCs in five-level hybrid ANPC topologies.

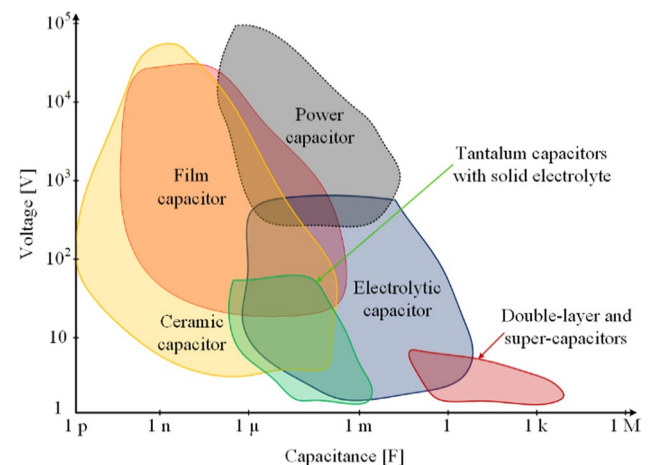


Fig. 5 Voltage ranges versus capacitance ranges of different types of capacitors [26]

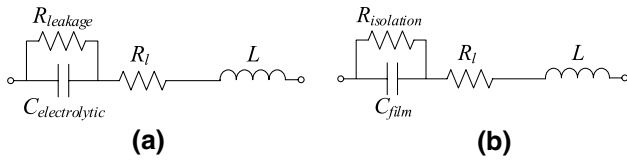


Fig. 6 Series-equivalent circuit model. **a** Electrolytic FC; **b** film FC

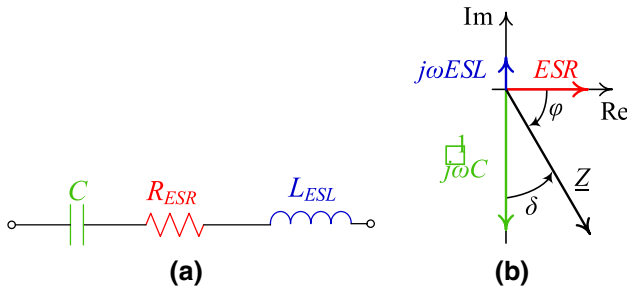


Fig. 7 FC representation. **a** Simplified Series-equivalent circuit **b** vector diagram

Figures 6 and 7 illustrate the electrical series-equivalent circuit models of both FCs. This model, which is the most commonly used, is rather simple, and gives a good frequency response [28], where $C_{\text{electrolytic}}$ and C_{film} are the capacitance of both electrolytic and film FCs, respectively. R_{leakage} and $R_{\text{isolation}}$ are the parallel-connected leakage current and isolation resistances, respectively. R_l and L are the series-connected resistance and inductance, respectively. Figure 6 can be simplified and represented in a vector diagram as shown in Fig. 7. It can be seen to be a serial combination of the equivalent series resistance (R_{ESR}) and the inductance (L_{ESL}). Finally, the capacitance can be estimated as in (5),

$$C = \begin{cases} C_{\text{electrolytic}} \cdot \left(1 + \frac{1}{C_{\text{electrolytic}}^2 \cdot R_{\text{leakage}}^2 \cdot \omega^2} \right) \\ C_{\text{film}} \cdot \left(1 + \frac{1}{C_{\text{film}}^2 \cdot R_{\text{isolation}}^2 \cdot \omega^2} \right) \end{cases} \quad (5)$$

where ω is the impedance (Z) angular frequency. In addition, both R_{ESR} and L_{ESL} can be calculated as in (6) and (7), respectively,

$$R_{\text{ESR}} = R_l + \frac{R_{\text{leakage}}}{1 + C_{\text{electrolytic}}^2 \cdot R_{\text{leakage}}^2 \cdot \omega^2} \quad (6)$$

$$L_{\text{ESL}} = L \quad (7)$$

It is worth noting that the dissipation factor ($\tan \delta$) is very important in film capacitors, since it measures the quality of resonance, as shown in Fig. 7b. Hence, the $\tan \delta$ is mentioned in most film capacitors datasheet instead of R_{ESR} . On the other hand, the electrolytic FC R_{ESR} increases when $C_{\text{electrolytic}}$ decreases. Therefore, film FCs are considered to be a better candidate for the HF operation of the five-level hybrid ANPC inverters.

FCs are responsible for generating the five-level V_{xn} in five-level hybrid ANPC inverter topologies. This is only achieved when the voltage across the FCs reaches $V_{\text{DC}}/4$. Several factors affect the amount of time required for FCs to reach their reference values, which include the switching frequency of the S_{x5-8} switching devices (f_c) and size of the FC.

As mentioned in Sect. 2, the S_{x5-8} switching devices are set to operate at a HF (i.e., $f_c = 30 \text{ kHz}$) to enhance the THD of the output three-phase current, which significantly reduces the ripple of the current. However, the size of the FC needs to be sufficiently large to limit the maximum voltage ripple ($\Delta V_{\text{FC,max}}$) that appears across it. This can be calculated as in (8):

$$\Delta V_{\text{FC,max}} = \frac{\max(D_{\text{FC}} \times I_{\text{FC}})}{C_{\text{FC}} \times 2 \times f_c} \quad (8)$$

where I_{FC} , D_{FC} , and C_{FC} are the FC, current duty cycle, and capacitance, respectively.

To simplify the design process, the worst-case scenario for $\Delta V_{\text{FC,max}}$ is considered and used to approximate the FC value as in (9):

$$\Delta V_{\text{FC,max(worst case)}} \approx \frac{I_{\text{pk}}}{C_{\text{FC}} \times 2 \times f_c} \quad (9)$$

where I_{pk} is the peak current at the full modulation index (MI). Therefore, the possible FC value is calculated as in (10):

$$C_{\text{FC}} = \frac{I_{\text{pk}}}{\Delta V_{\text{FC,max(worst case)}} \times 2 \times f_c} \quad (10)$$

Assuming the maximum voltage ripple does not exceed the 20 V of the steady-state value of the V_{FC} voltage at full values of the MI and the rated power, C_{FC} is set as in (11):

$$C_{\text{FC}} \geq \frac{34.5\text{A}}{20\text{V} \times 2 \times 30\text{kHz}} \geq 28.75 \mu\text{F}. \quad (11)$$

4 Simulation verification

Comprehensive simulation results obtained from the PSIM Simulation Tool are presented in this section. The effectiveness of proper FC selection is evident in the performance of the five-level hybrid ANPC inverter during HF operation. The system parameters are listed in Table 2. In this study, f_c was set as low as 1.5 kHz. Meanwhile, it was set to 30 kHz for HF operation. In addition, the fundamental frequency was maintained at 60 Hz during all of the operations.

The simulation results shown in Fig. 8 were used to evaluate the performance of the five-level hybrid ANPC during LF and HF operations using two different capacitors. From Fig. 8a, b it can be seen that the 220 μF electrolytic FC has better performance than the 30 μF film FC at $f_c = 1.5$ kHz. However, the 220 μF electrolytic FC has a slower startup control to form a five-level output voltage. In addition, LF operation degrades the system performance due to the high distortions in the output current and voltage.

To improve the system performance, f_c was increased from 1.5 to 30 kHz, as shown in Fig. 8c and Fig. 8d. During HF operation, the 30 μF film FC outperformed the 220 μF electrolytic FC. This is due to the natural material of the film capacitor and its small capacitance. As a result, the three-phase FCs reached their reference value (i.e., 75 V) in only 0.7 s due to the fast charging and discharging capability of the film capacitor.

The magnified simulation results of Fig. 6 with additional analysis are shown in Fig. 9. From Fig. 9a, it can be seen that the 220 μF electrolytic FC resulted in the full formation of the five-level output voltage (V_{an}). However, a high THD was obtained during LF operation. A Fast Fourier transform (FFT) analysis of I_a shows that the distortion is high when $f_c = 1.5$ kHz. If the 220 μF electrolytic FC is replaced by the 30 μF film FC during LF operation, more distortion occurs

in addition to the high voltage ripple across the FCs, as shown in Fig. 9b.

Nevertheless, when $f_c = 30$ kHz, the THD of I_a is significantly reduced when using either FC type. When using the 220 μF electrolytic FC, the performance is similar to that of a three-level hybrid ANPC, as shown in Fig. 9c. This is due to the slow charging and discharging properties of this type of FC. Consequently, a higher THD of V_{an} is obtained. To enhance the performance of five-level hybrid ANPC inverters during HF operation, a film FC was used instead of an electrolytic FC. As shown in Fig. 9d, V_{an} and V_{ab} were fully formed at the five and nine levels. In addition, the three-phase FC voltages were regulated at 75 V. Moreover, the THD of the three-phase output current was minimized to 0.41%, which is excellent and desirable in many industrial applications.

To further investigate the performances of the 220 μF electrolytic and 30 μF film FCs, comparative charts are presented in Fig. 10. These charts indicate that the 30 μF film FC is slightly better than the 220 μF electrolytic FC in terms of minimizing the THD of the three-phase output current during HF operation. In addition, a significant reduction in the THD of V_{an} during various operations was observed, which includes variations in MI and f_c , particularly in the low MI and HF ranges, as shown in Fig. 10b.

5 Experimental validation

Validation of the proposed 30 μF film FC for enhancing the five-level hybrid ANPC inverter performance in HF operation was extensively demonstrated by some experiments comparing it with the 220 μF electrolytic FC. Using an electrolytic FC with a small capacitance (i.e., ~ 30 μF) would result in very poor system performance, and might lead to serious damage of the capacitor, and unbalanced voltages across the FC due to its small capacitance and large ESR. Therefore, two different types of FCs (i.e., 30 μF film and 220 μF electrolytic) were used in experimental trials at $f_c = 30$ kHz. As shown in Fig. 11, these experiments were performed using a five-level hybrid ANPC inverter and a TMS320f28377s digital signal processor (developed by Texas Instruments) that was operated as the main control board for executing the experimental code in a code composer studio environment. LF was excluded from the experimental verification due to the large ripples present across the FCs, as shown in Fig. 9a and Fig. 9b. Therefore, f_c was fixed at 30 kHz during experimental trials. In addition, a resistor was used to ensure that the FCs were fully discharged before each experiment. Table 3 presents a detailed list of

Table 2 System parameters

Item, symbol	Value [unit]
DC-link voltage, V_{DC}	300 [V]
DC-link capacitance, C_1, C_2	4700 [μF]
Film FC capacitance, C_{film}	30 [μF]
Electrolytic FC capacitance, $C_{\text{electrolytic}}$	220 [μF]
Film FC rated voltage	250 [V]
Electrolytic FC rated voltage	400 [V]
Load resistance, R	10 [Ω]
Load inductance, L	2 [mH]
Fundamental frequency, f_o	60 [Hz]
PWM carrier frequency, f_c	1.5, 30 [kHz]

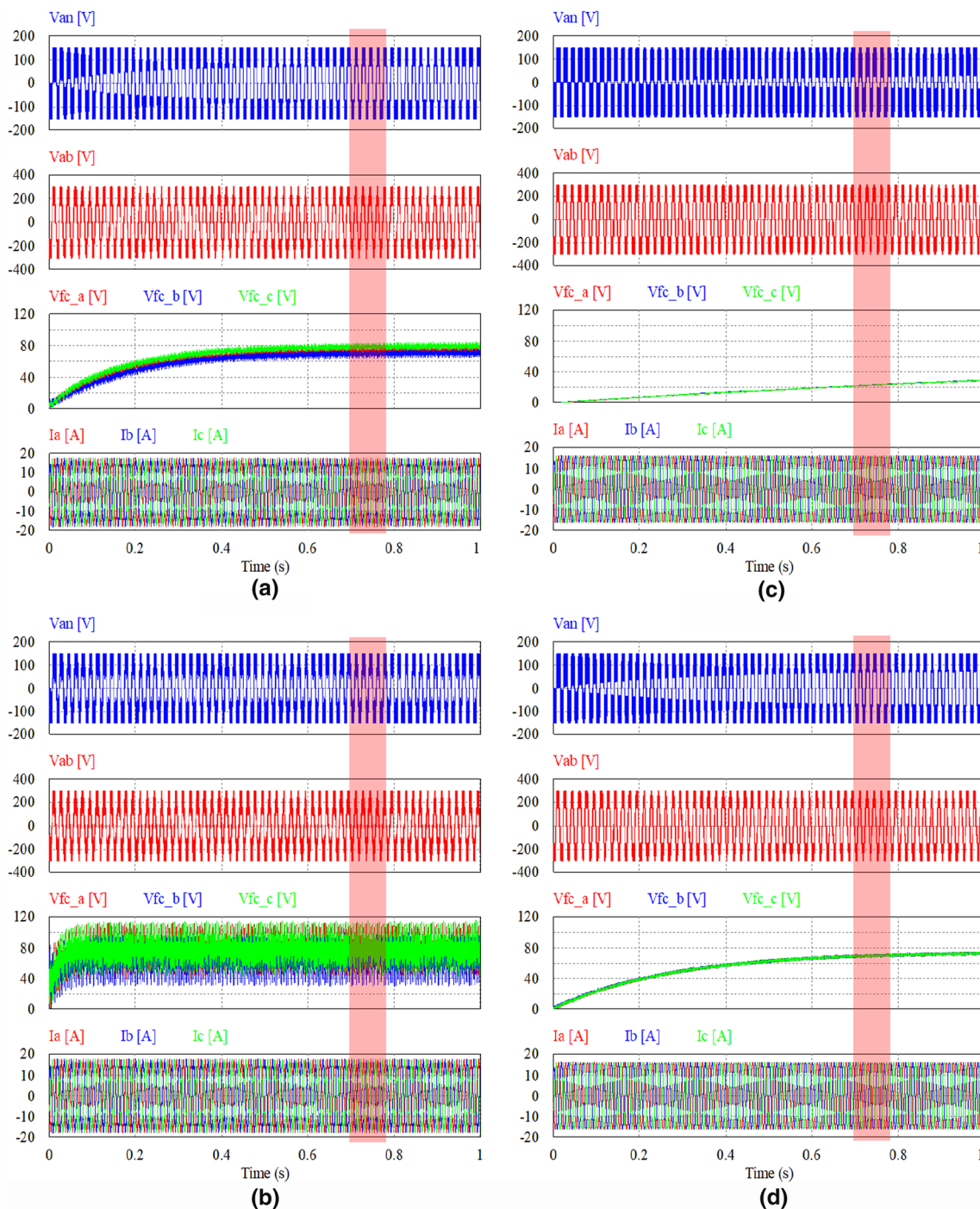


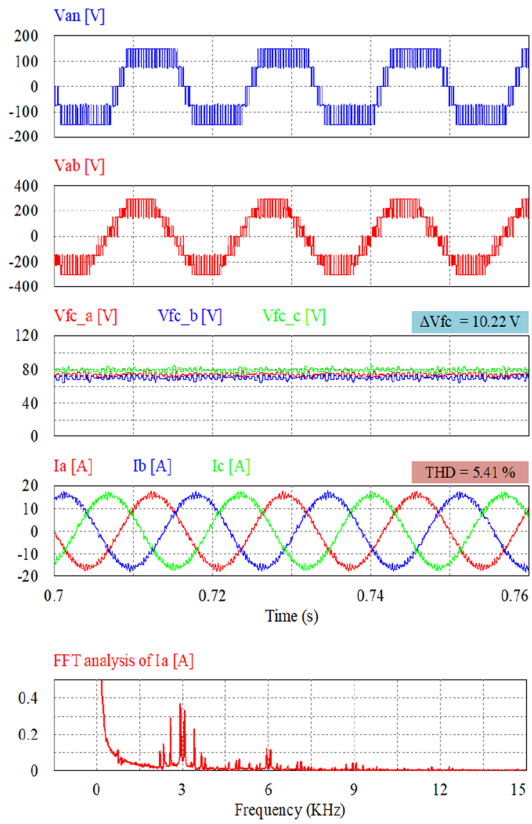
Fig. 8 Simulation performance evaluation results of a five-level hybrid ANPC inverter under two types of FC at low and high PWM switching frequencies. **a** 220 μF electrolytic FC at $f_c=1.5$ kHz; **b**

30 μF film FC at $f_c=1.5$ kHz; **c** 220 μF electrolytic FC at $f_c=30$ kHz; **d** 30 μF film FC at $f_c=30$ kHz

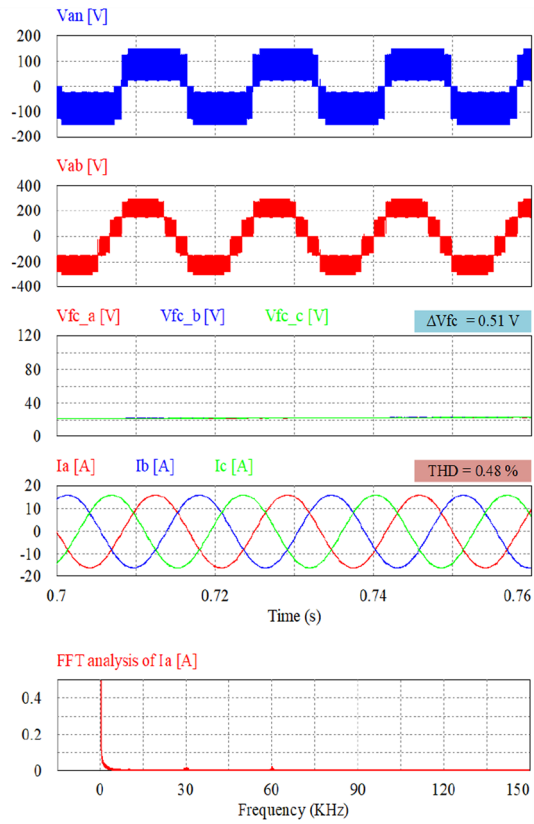
the 220 μF electrolytic and 30 μF film FCs used in this study. This table shows that the 30 μF film FCs outperformed the 220 μF electrolytic FCs in terms of many features, including size, price, and reliability in the HF range. In addition, the

very low ESR of the 30 μF film FC resulted in a very long lifespan when compared to the 220 μF electrolytic.

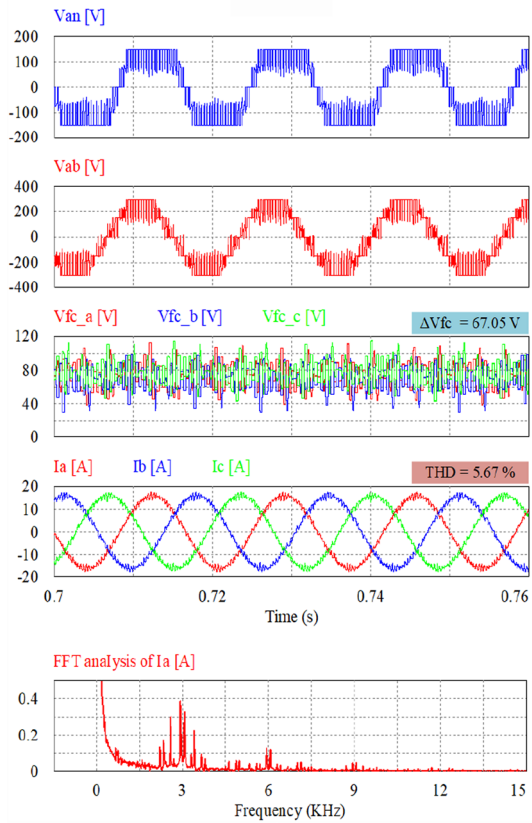
Figure 12 shows experimental results for the performance evaluation of a five-level hybrid ANPC inverter using



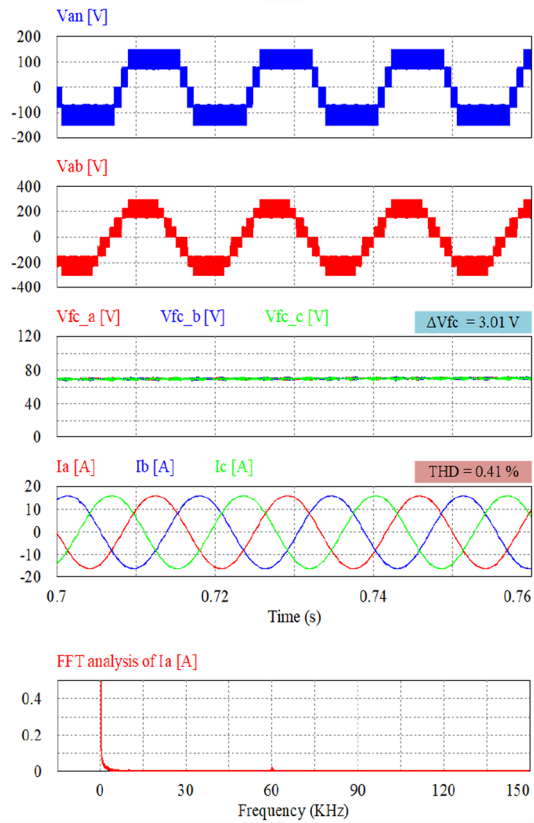
(a)



(c)



(b)



(d)

Fig. 9 Magnified simulation performance evaluation results of a five-level hybrid ANPC inverter under two types of FC at low and high PWM switching frequencies. **a** 220 μF electrolytic FC at $f_c = 1.5 \text{ kHz}$; **b** 30 μF film FC at $f_c = 1.5 \text{ kHz}$; **c** 220 μF electrolytic FC at $f_c = 30 \text{ kHz}$; **d** 30 μF film FC at $f_c = 30 \text{ kHz}$

a 220- μF electrolytic FC at $f_c = 30 \text{ kHz}$ with two different zones for the magnified results. This figure shows that the five-level hybrid ANPC inverter cannot operate as desired to form a V_{an} with five discrete levels. As a result, a high THD of V_{an} was observed, particularly in zone-1. In zone-2, the performance of the system was similar to that of zone-1 with a 1 s of delay for charging the 220 μF electrolytic FC. Therefore, this type of FC requires a very long time to ensure that the five-level hybrid ANPC inverter operates as desired.

Consequently, the performance of the five-level hybrid ANPC inverter was improved when a 30 μF film FC was used. Due to its physical properties when operating in HF applications and under a small capacitance, the charging capability was very quick when compared to that of the 220 μF electrolytic FC. As a result, a considerably better performance was achieved, as shown in Fig. 13. Initially,

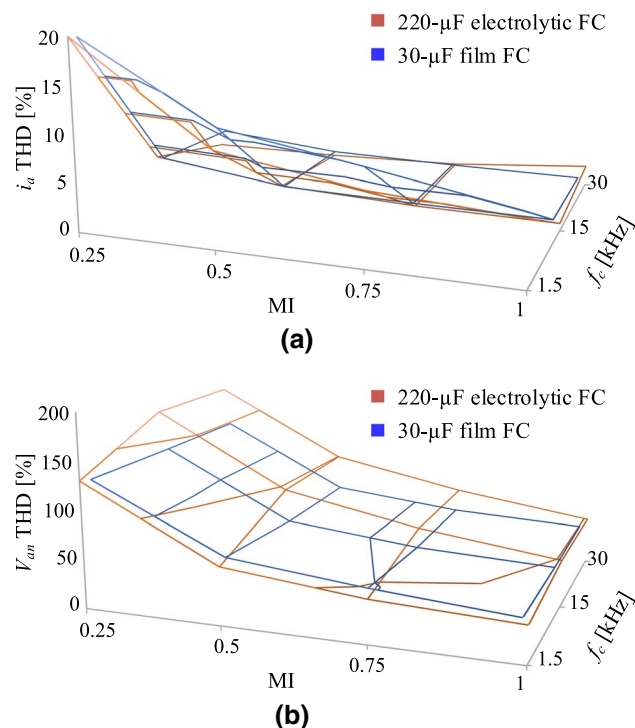


Fig. 10 Simulation comparison for different values of f_c and MI. **a** THD of i_a ; **b** THD of V_{an}

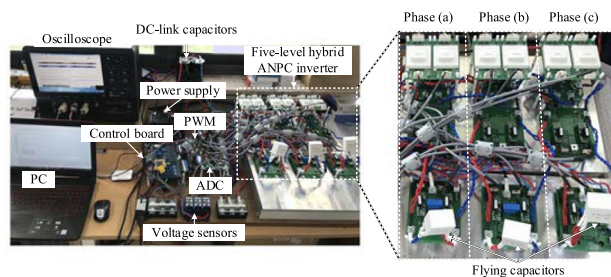


Fig. 11 Experimental setup of a five-level hybrid ANPC inverter

the 30 μF film FC was fully discharged at the startup of the five-level hybrid ANPC inverter, as shown in Fig. 13a. After 1 s of natural quick charging, the performance of the five-level hybrid ANPC inverter was as desired, as shown in Fig. 13b. As a result, the V_{an} THD was minimized, as shown in Fig. 12. Hence, the 30- μF film FC is strongly recommended for enhancing the performance of five-level hybrid ANPC inverters.

6 Conclusion

In this study, a novel and comprehensive analysis was presented for the proper selection of a FC for the performance enhancement of a five-level hybrid ANPC inverter. Among the different FC types, the film FC was recommended due to its excellent operation, particularly in the HF range. Extensive simulations and experiments were conducted to verify its effectiveness in improving the overall performance of a five-level hybrid ANPC inverter. When compared to electrolytic FCs, film FCs significantly enhanced the capability of the system for five-level operating performance with low THD values in the output pole voltage and phase current. Hence, the required filter size can be reduced when it is implemented in various applications. Therefore, film FCs are desirable for enhancing the operation of five-level hybrid ANPC inverters, particularly in the HF range.

Table 3 Experimental FC Specifications [29, 30]

Item [unit]	Electrolytic	Film
Design		
Supplier	KEMET	KEMET
Series	ALS30	C4AT
Part number	ALS30A221DA400	C4ATDBW5300A30J
Type	Aluminum	Film
Dielectric	Aluminum electrolytic	Metallized polypropylene
Style	Screw terminal	Radial
Polarity	Yes	No
Capacitance [μF]	220	30
Capacitance tolerance [%]	20	5
DC voltage [V]	400	250
Surge voltage [V]	440	500
Maximum temperature [$^{\circ}\text{C}$]	85	85
Minimum temperature [$^{\circ}\text{C}$]	-40	-40
Maximum dv/dt [$\text{V}/\mu\text{s}$]	-	20
Current ripple [A]	4.4 at 10 kHz, 85 $^{\circ}\text{C}$	22 at 100 kHz, 70 $^{\circ}\text{C}$
ESR [$\text{m}\Omega$]	387 at 10 kHz 20 $^{\circ}\text{C}$	2.6 at 100 kHz
Shelf life [Year]	3	Unlimited
Lifespan [h]	11,000	100,000
Environment	Harmful	Friendly
End life	Explosion	Soft
Length [mm]	52	42.5
Weight [g]	75	76.94
Lead	Screw terminals	4-wire leads
Cost [US\$]	13.77	10.39

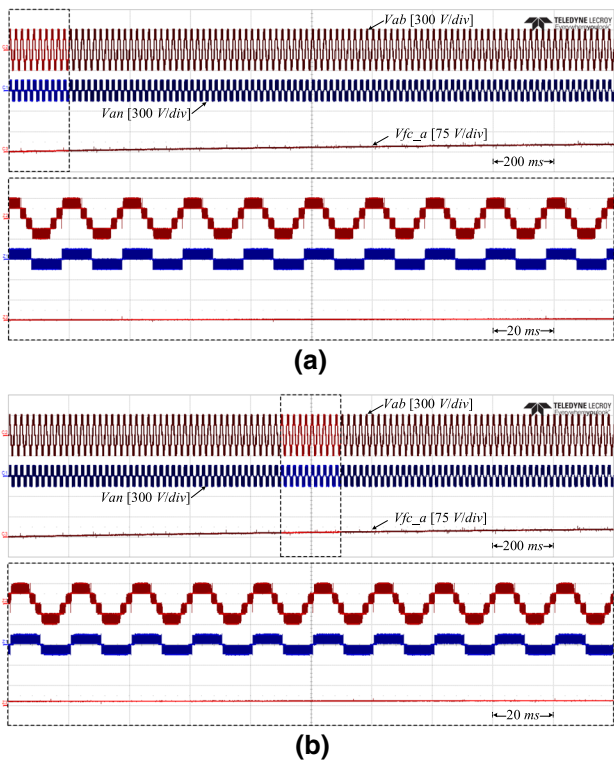


Fig. 12 Experimental results for a performance evaluation of a five-level hybrid ANPC inverter using a 220 μF electrolytic FC at $f_c = 30$ kHz: magnified zones **a** 1; **b** 2

Acknowledgements This work was supported by Korea Electric Power Corporation, the Korea Institute of Energy Technology Evaluation and Planning (KETEP) and the Ministry of Trade, Industry & Energy (MOTIE) of the Republic of Korea (No. R21X001-11 and No. 20206910100160).

References

1. Kouro, S., et al.: Recent advances and industrial applications of multilevel converters. *IEEE Trans. Ind. Electron.* **57**(8), 2553–2580 (2010)
2. Abu-Rub, H., Holtz, J., Rodriguez, J., Ge, B.: Medium-voltage multilevel converters—state of the art, challenges, and requirements in industrial applications. *IEEE Trans. Ind. Electron.* **57**(8), 2581–2596 (2010)
3. Rodriguez, J., Bernet, S., Steimer, P., Lizama, I.: A survey on neutral-point-clamped inverters. *IEEE Trans. Ind. Electron.* **57**(7), 2219–2230 (2010)
4. Sathyaseelan, B., Vijay Shankar, S., Suresh, K., et al.: Design and implementation of comprehensive converter. *J. Electr. Eng. Technol.* **16**, 3093–3101 (2021)
5. Dwivedi, A., Pahariya, Y.: Design and analysis of hybrid multilevel inverter for asymmetrical input voltages. *J. Electr. Eng. Technol.* **16**, 3025–3036 (2021)
6. Lee, K.-B., Lee, J.-S.: *Reliability improvement technology for power converters*. Springer, Singapore (2017)

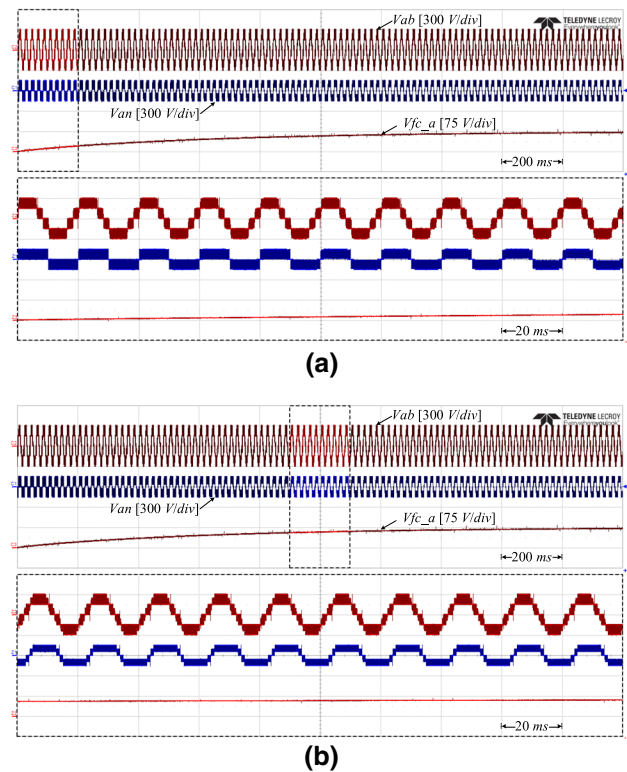
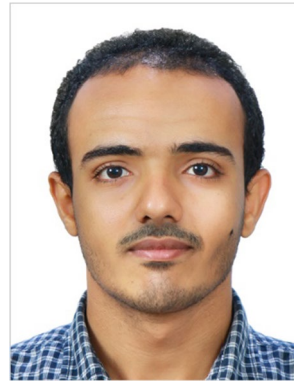


Fig. 13 Experimental results for a performance evaluation of a five-level hybrid ANPC inverter using a 30 μF film FC at $f_c = 30$ kHz: magnified zones **a** 1; **b** 2

7. Guan, Q., et al.: An extremely high efficient three-level active neutral-point-clamped converter comprising SiC and Si hybrid power stages. *IEEE Trans. Power Electron.* **33**(10), 8341–8352 (2018)
8. Song, M.-G., Kim, S.-M., Lee, K.-B.: Independent switching technique to remove abnormal output voltage in hybrid active NPC inverters. *J. Power Electron* **21**, 85–93 (2021)
9. Halabi, L.M., Alsofyani, I.M., Lee, K.-B.: Hardware implementation for hybrid active NPC converters using FPGA-based dual pulse width modulation. *J. Power Electron* **21**, 1669–1679 (2021)
10. Sivasubramanian, M., Boopathi, C.S.: A switched capacitor based seven level active neutral point clamped (ANPC) inverter topology with reduced switching devices. *J. Electr. Eng. Technol.* **16**, 3103–3112 (2021)
11. Jo, H.-R., Kim, Y.-J., Lee, K.-B.: LCL-Filter design based on modulation index for grid-connected three-level hybrid ANPC inverters. *J. Electr. Eng. Technol.* **16**, 1517–1525 (2021)
12. P Barbosa P Steimer J Steinke L Meysenc M Winkelkemper N Celanovic 2005 Active neutral-point-clamped (ANPC) multilevel converter technology *Proc Eur Conf Power Electron. Appl* 1 10
13. F Kieferndorf M Basler LA Serpa JH Fabian A Coccia GA Scheuer 2010 A new medium voltage drive system based on ANPC-5L technology *Proc Int Conf Ind Technol.* 643 649
14. Jiang, L., et al.: SVPWM algorithm for five-level active-neutral-point-clamped H-bridge inverters. *J. Power Electron.* **21**, 1123–1134 (2021)
15. Zhou, D., Ding, L., Li, Y.: Two-stage optimization-based model predictive control of 5L-ANPC converter-fed PMSM drives. *IEEE Trans. Ind. Electron.* **68**(5), 3739–3749 (2021)

16. Narimani, M., Wu, B., Zargari, N.R.: A novel five-level voltage source inverter with sinusoidal pulse width modulator for medium-voltage applications. *IEEE Trans. Power Electron.* **31**(3), 1959–1967 (2016)
17. Dekka, A., Narimani, M.: Capacitor voltage balancing and current control of a five-level nested neutral-point-clamped converter. *IEEE Trans. Power Electron.* **33**(12), 10169–10177 (2018)
18. Hafez, A.A., Mahmoud, A.A., Yousef, A.M.: Robust and intelligent control for single-stage grid-connected modular multilevel converter in PV applications. *J. Electr. Eng. Technol.* **16**, 917–931 (2021)
19. Wang, K., Zheng, Z., Xu, L., Li, Y.: An optimized carrier-based PWM method and voltage balancing control for five-level ANPC converters. *IEEE Trans. Ind. Electron.* **67**(11), 9120–9132 (2020)
20. Pulikanti, S., Agelidis, V.: Hybrid flying-capacitor-based active neutral-point-clamped five-level converter operated with SHE-PWM. *IEEE Trans. Ind. Electron.* **58**(10), 4643–4653 (2011)
21. Shukla, A., Ghosh, A., Joshi, A.: Natural balancing of flying capacitor voltages in multicell inverter under PD carrier-based. *IEEE Trans. Power Electron.* **26**(6), 1682–1693 (2011)
22. Ghias, A.M.Y.M., Pou, J., Ciobotaru, M., Agelidis, V.G.: Voltage balancing method using phase-shifted PWM for the flying capacitor multilevel. *IEEE Trans. Power Electron.* **29**(9), 4521–4531 (2014)
23. Wang, K., Li, Y.D., Zheng, Z.D., Xu, L., Ma, H.W.: Self-precharge of floating capacitors in a five-level ANPC inverter. *Proc. 7th Power Electron. Motion Control Conf.* **3**, 1776–1780 (2012)
24. Terzulli, G. 2010. Film technology to replace electrolytic technology in wind power applications. *AVX Tech. Note*
25. Kim, S.-H. 2017 *Electric motor control. DC, AC, and BLDC motors.* Elsevier
26. Sayyad, J., Nasikkar, P., Singh, A.P., Ozana, S.: Capacitive load-based smart OTF for high power rated SPV module. *Energies* **14**, 788 (2021)
27. Streibl, M., Karmazin, R., Moos, R.: Materials and applications of polymer films for power capacitors with special respect to nanocomposites. *IEEE Trans. Dielectr. Electr. Insul.* **25**(6), 2429–2442 (2018)
28. Abdennadher, K., Venet, P., Rojat, G., Retif, J.-M.: A real time predictive maintenance system of aluminum electrolytic capacitors used in uninterrupted power supplies. *Proc. IEEE Ind. Appl. Soc. Conf.* **46**(1), 1644–1652 (2008)
29. KEMET 2021 Screw terminal aluminum electrolytic capacitors. ALS30/31 datasheet
30. KEMET 2022 Printed circuit board mount power film capacitors. C4AQ datasheet.

Springer Nature or its licensor holds exclusive rights to this article under a publishing agreement with the author(s) or other rightsholder(s); author self-archiving of the accepted manuscript version of this article is solely governed by the terms of such publishing agreement and applicable law.



Samer Saleh Hakami received the B.S. (Hons) degree in Electrical Engineering from the Universiti Tun Hussein Onn Malaysia, Johor, Malaysia, in 2016; and the M.S. degree in Electrical and Computer Engineering from Ajou University, Suwon, Korea, in 2020, where he is presently working toward the Ph.D. degree in Electrical and Computer Engineering. His current research interests include multilevel inverters, advanced motor drives, and the reliability of power converters.



Kyo-Beum Lee received the B.S. and M.S. degrees in Electrical and Electronic Engineering from the Ajou University, Suwon, Korea, in 1997 and 1999, respectively. He received the Ph.D. degree in Electrical Engineering from the Korea University, Seoul, Korea, in 2003. From 2003 to 2006, he was with the Institute of Energy Technology, Aalborg University, Aalborg, Denmark. From 2006 to 2007, he was with the Division of Electronics and Information Engineering, Jeonbuk National University, Jeonju, Korea. In 2007, he joined the Department of Electrical and Computer Engineering, Ajou University, Suwon, Korea. He is an Editor-in-Chief of the *Journal of Power Electronics*. He is an Associated Editor of the *IEEE Transactions on Power Electronics*. His current research interests include electric machine drives, renewable power generations, and electric vehicle applications.